Electronic Supplementary Material (ESI) for Journal of Materials Chemistry A.

Supporting Information

Enhanced Ionic transport in ferroelectric polymer fiber mats

Ayesha Sultana, Md. Mehebub Alam, Simone Fabiano, Xavier Crispin, Dan Zhao**

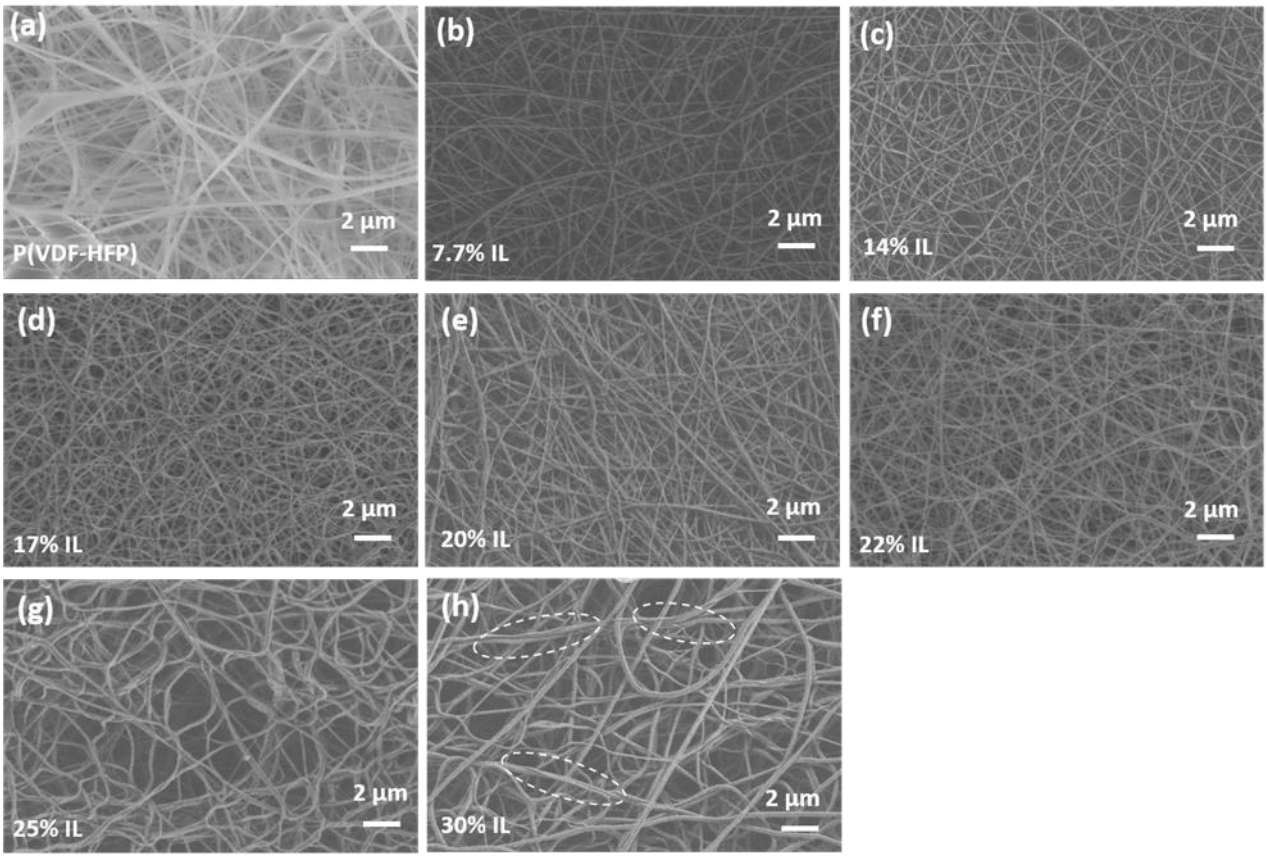

Fig. S1 FE-SEM images of (a) pure P(VDF-HFP), (b) 7.7%, (c) 14%, (d) 17 %, (e) 20 % (f) 22%, (g) 25% and (h) 30% IL content electrospun fiber. The aggregation of fibers for 30% IL is marked in (h).

Note S1. **The analyzation of the FT-IR spectroscopy**

To quantify the total electroactive phase the equation used is

$$F_{EA} = \frac{A_{EA}}{\frac{K_{841}}{K_{764}}A_{764}+A_{EA}} \times 100\% \qquad \text{(S1)}$$

where A_{EA}, A_{764} are absorbance intensities at 841 and 764 cm^{-1} respectively, $K_{841}$and K_{764} are the corresponding absorption coefficients.[S1, S2]

The relative amount of β-phase is calculated by equation

$$F_{\beta} = F_{EA} \times \frac{A_{\beta}}{A_{\beta}+A_{\gamma}} \qquad \text{(S2)}$$

where A_{β}, A_{γ} are absorbance intensities at 1275 and 1234 cm^{-1} respectively.[S1, S2]

For the fibers as there is no presence of γ-phase the total electroactive phase is considered as the polar β-phase content.

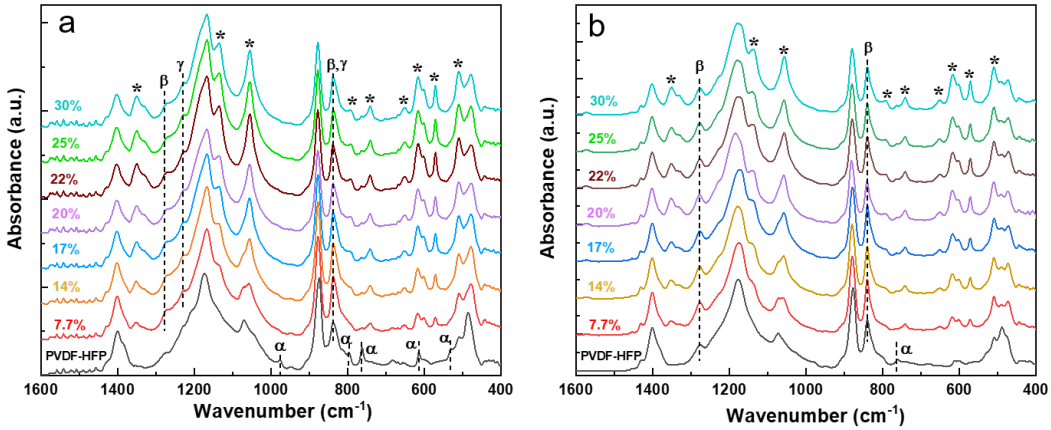

Fig. S2 FT-IR spectra of (a) solution casted films and (b) electrospun fibers with different IL content. The absorption bands for the IL are marked (*) in the spectra.

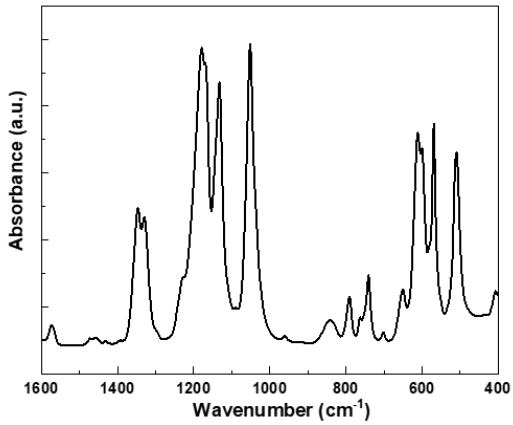

Fig. S3 FT-IR spectra of pure EMIM TFSI in the wavenumber range from 400 cm^{-1} to 1600 cm^{-1}.

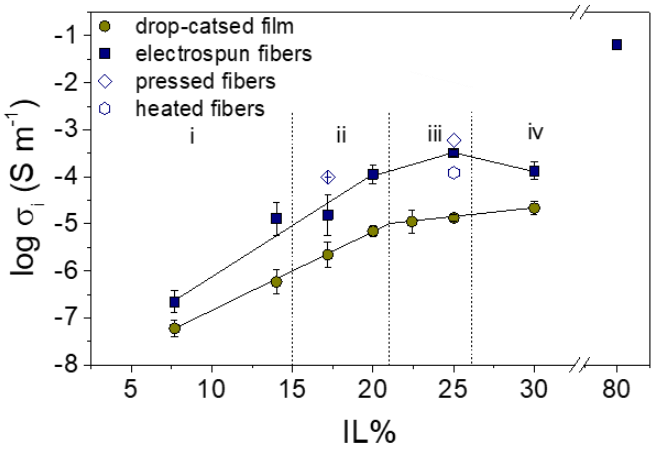

Fig. S4 Ionic conductivity of the P(VDF-HFP) based electrospun fiber mats (solid blue squares) and drop casted films (solid yellow dots) containing the same IL percentage at room temperature.

Note S2. **Porosity measurement and calculation**

The porosity of the fiber mats was calculated as reported.[S3] First, the electrospun fiber mats were soaked in 2-propanol. Then the wet fiber mat was taken out and put on a scale after gently removing the excess 2-propanol from the surface by cloth wipes. The weight of the fiber mat decreased with time due to the evaporation of 2-propanol and was stable after some time. The initial and final weight of the fiber mat was noted. The porosity was calculated using the equation,

$$Porosity = \frac{pore\ volume}{total\ volume} = \frac{\frac{m_{in}-m_f}{\rho_{pr}}}{\frac{m_{in}-m_f}{\rho_{pr}}+\frac{m_f}{\rho_{hfp}}} \qquad \text{(S3)}$$

Where, m_{in} and m_f are initial and final mass of the fiber mat. ρ_{pr} and ρ_{hfp} are density of 2-propanol and P(VDF-HFP).

Note S3. The conductivity and molar conductivity

The ionic conductivity of all the samples are measured by frequency dependent impedance spectroscopy. The real part, imaginary part and the phase angle was measured when the

frequency scan from 1M Hz to 1 Hz at fixed temperature. The resistance (R) of a sample was considered as the real impedance at high frequency when the phase angle is the closest to zero.[S4] Hence, the ionic conductivity (σ_i) can be calculated from $\sigma_i = \frac{L}{RA}$, in which L represent the distance between the two electrodes (the thickness of the sample) and A is the area of the electrode.

The molar conductivity (Λ) is calculated by dividing the conductivity with the molar concentration per volume of the ionic liquid (c_{IL}):

$$c_{IL} = \frac{1}{\frac{M_{IL}}{\rho_{IL}} + \frac{M_{IL}\frac{1-f_{IL}}{f_{IL}}}{\rho_{po}}} \qquad \text{(S4)}$$

$M_{IL}$is the molar mass of the ionic liquid, ρ_{IL} and $\rho_{po}$are the density of the ionic liquid and polymer, $f_{IL}$is the weight percentage of the ionic liquid. For fiber mats, the molar concentration is multiplied with the solid content percentage (1-porosity%).

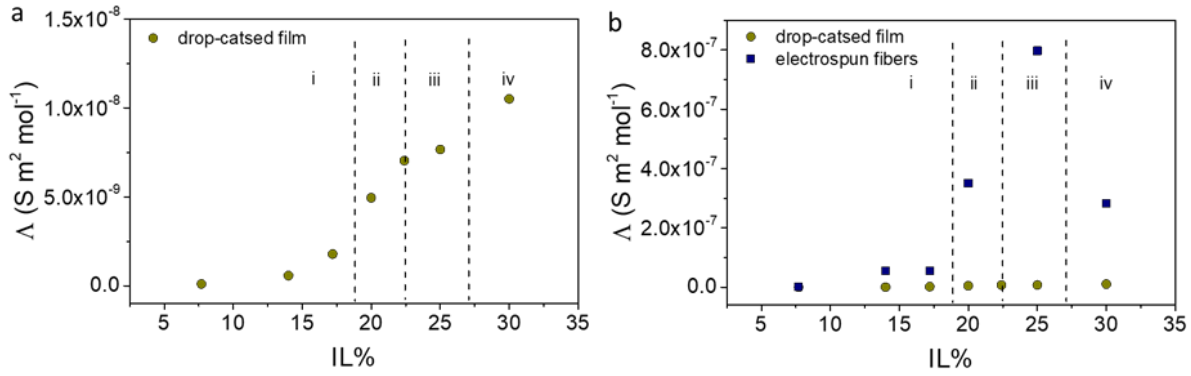

Fig. S5 The linear scale plot of the molar conductivity of the films and fiber mats.

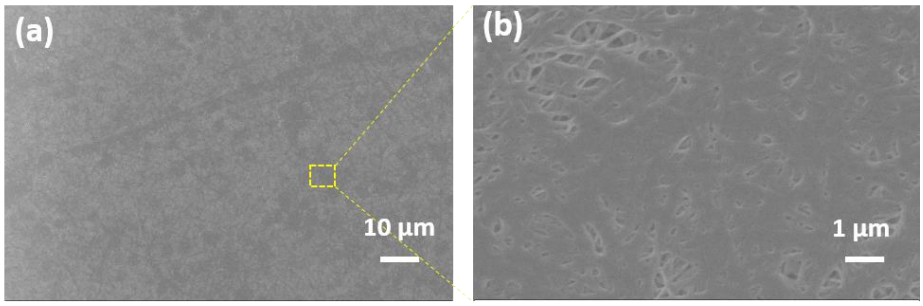

Fig. S6 FE-SEM images of 25% IL cold pressed electrospun fiber in (a) low magnification and (b) high magnification.

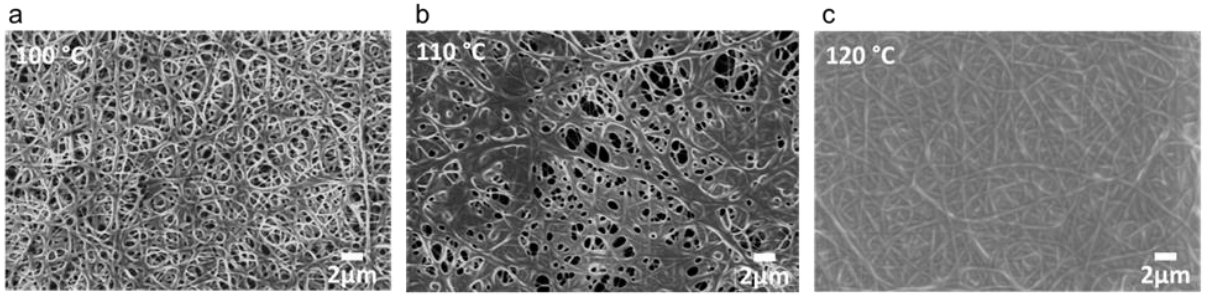

Fig. S7 The 25% IL containing fiber mat was heated at different temperature to loss the porosity completely. FE-SEM images of electrospun fiber mats containing 25% of IL heated at (a) 100°C, (b) 110°C and (c) 120°C. It is clear that the porosity decreased after heating at 120°C.

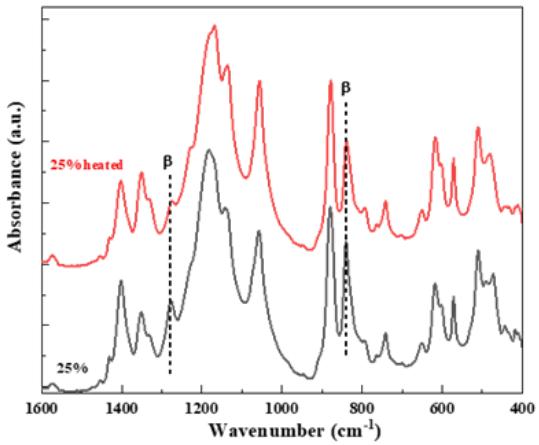

Fig. S8 FT-IR spectra of 25% IL containing electrospun fiber before and after heating at 120°C. The peak intensity corresponding to ferroelectric β-phase is significantly decreased after heating.

Note S4. **The piezoelectric characterization**

The piezoelectric measurements are carried out using the same devices as for ionic conductivity measurements. The output voltage of all the samples were measured by applying the same force a force in a frequency of 3 Hz. The piezoelectric output voltage of 2.5 V is obtained from pure P(VDF-HFP) fiber mats (Fig. S9a). The curve of the open voltage response follows the shape of typical piezoelectric response of sharp peak. Addition of 7.7% IL decreased the output voltage by one order of magnitude as the piezo-response is partially screened by the ions (Fig. S9b). The screening effect become more dominating with the increase of IL content thus the device with 14% IL delivered a piezoelectric voltage of only 0.1 V (Fig. S9c). It should be mentioned that ionic liquid can soften the fiber mats, which would lead to larger deformation of the sample in the direction of the applied force. However, the force applied to the PVDF phase that is in response for the piezoelectricity might reduce with increasing IL contents. We have increased the applied force to test if PVDF could show piezoelectric response. As shown in Fig. S11, there are still no obvious piezoelectric response when the force increased to 40 N. Moreover, the range of ionic liquid content in this study is within the "polymer electrolyte", which usually contains less than 40% liquid electrolyte in P(VDF-HFP) based composite electrolytes.[S5] According literature, the Young's module of the same P(VDF-HFP)/IL composite decrease to half when IL content changed from 13% to 26%.[S6] The shape of the pressure-induced voltage response in the one with 25% IL fiber mats is completely different from typical piezoelectric response of the sample containing 14% IL (as shown in inset figures in S9). Similar response for 20% and 30% IL containing devices (Fig. S9d and S9f) are also observed. Thus, we believed that the decrease in piezoelectric response is mostly due to screening effect as discussed in the manuscript. More detailed studies is needed to quantitatively describe piezoelectric and ionic screening effect.

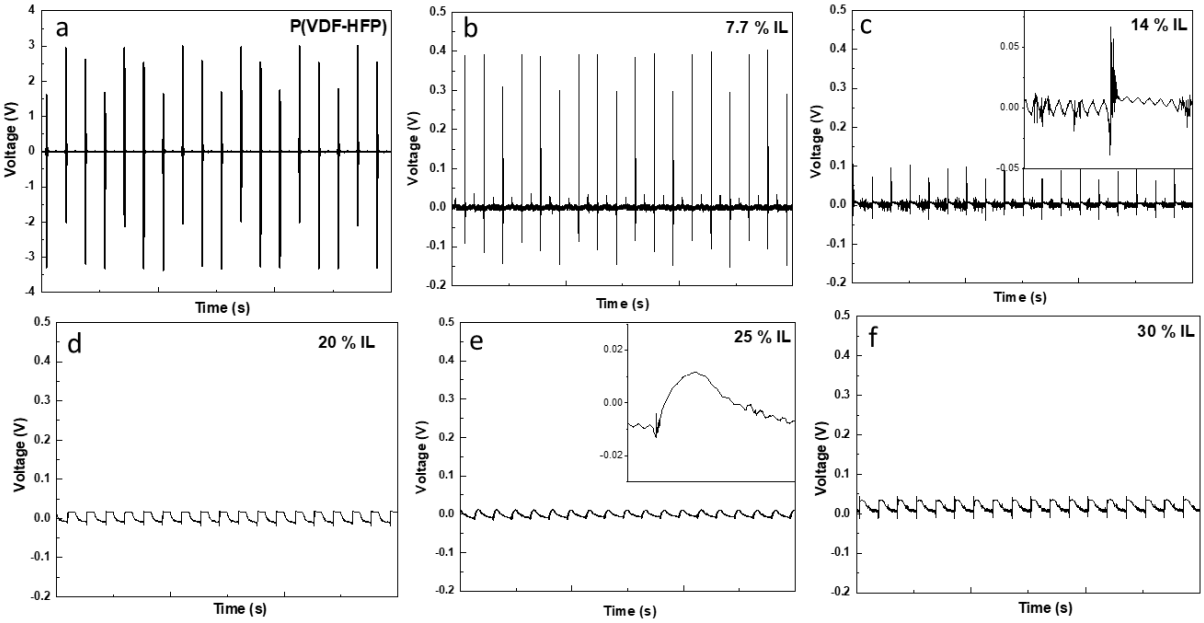

Fig. S9 Piezoresponse from electrospun (a) P(VDF-HFP), (b) 7.7% IL, (c) 14% IL, (d) 20% IL, (e) 25% IL, (f) 30% IL fiber based devices. The time scale is 0.3 s for both of the inset figures.

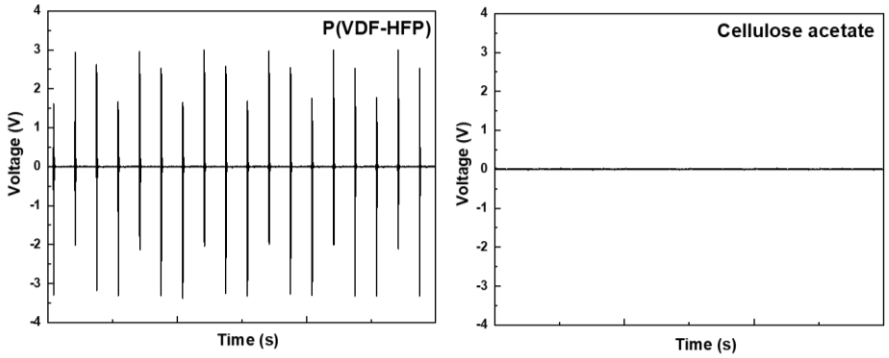

Fig. S10 Comparison of output voltage response of P(VDF-HFP) and cellulose acetate fiber mat-based device under same experimental condition.

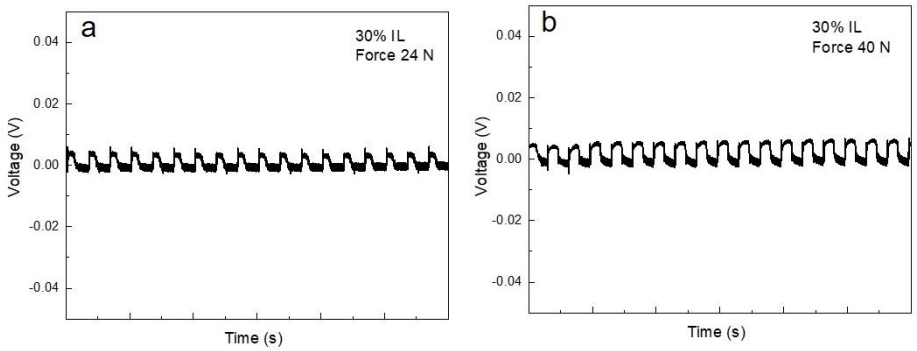

Fig. S11 Piezoelectric response from 30% IL fiber-based device under applied force of (a) 24 N and (b) 40 N.

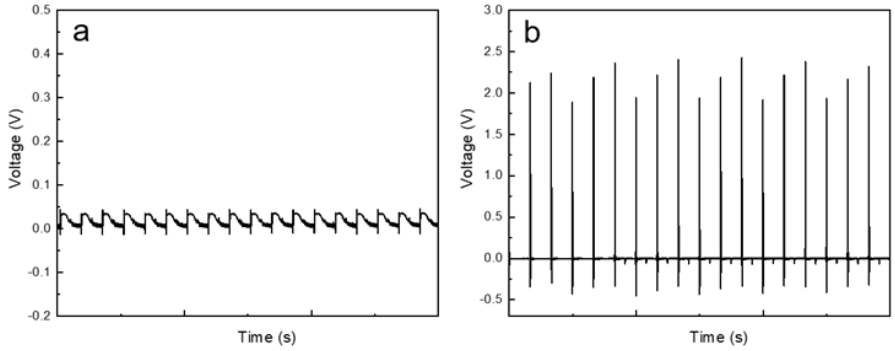

Fig. S12 Piezoelectric response from 30% IL fiber-based device (a) before and (b) after removing IL from fiber mat.

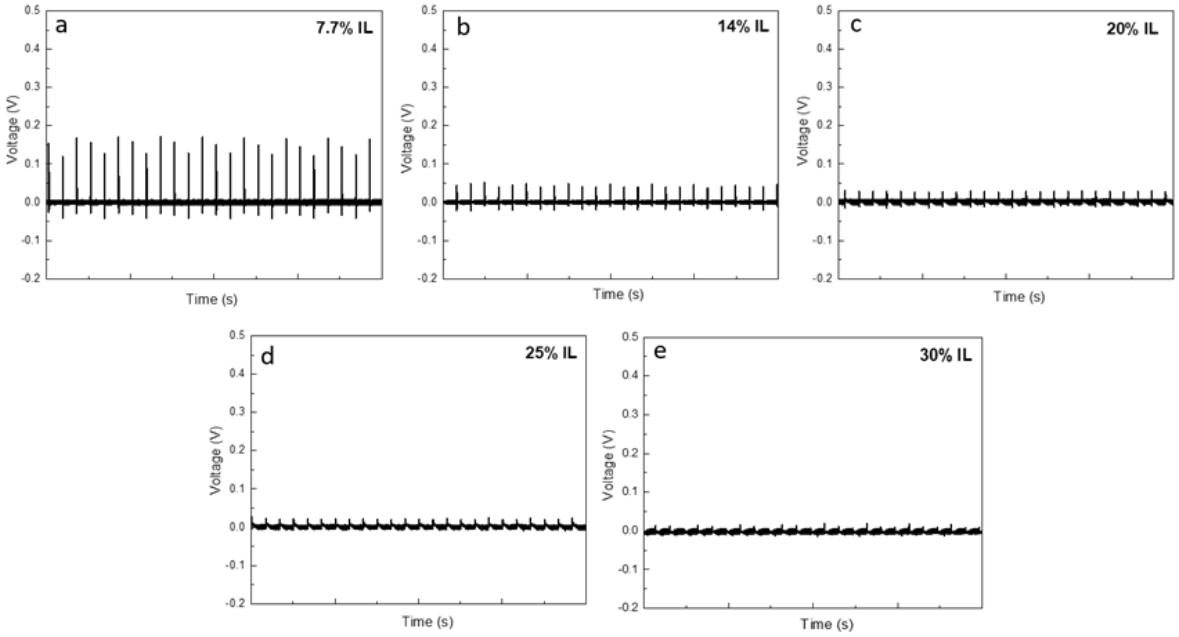

Fig. S13 Piezoelectric response from (a) 7.7% IL, (b) 14% IL, (c) 20% IL, (d) 25% IL and (e) 30% IL content drop-casted films based device.

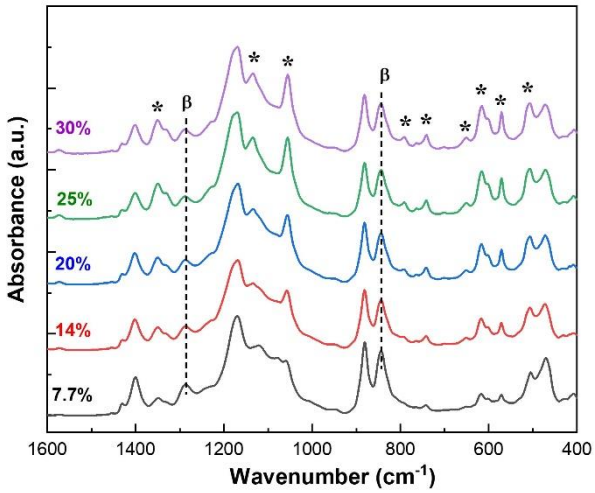

Fig. S14 The FT-IR spectra P(VDF-TrFE) based solution casted films with different IL content. The absorption bands for the IL are marked (*) in the spectra.

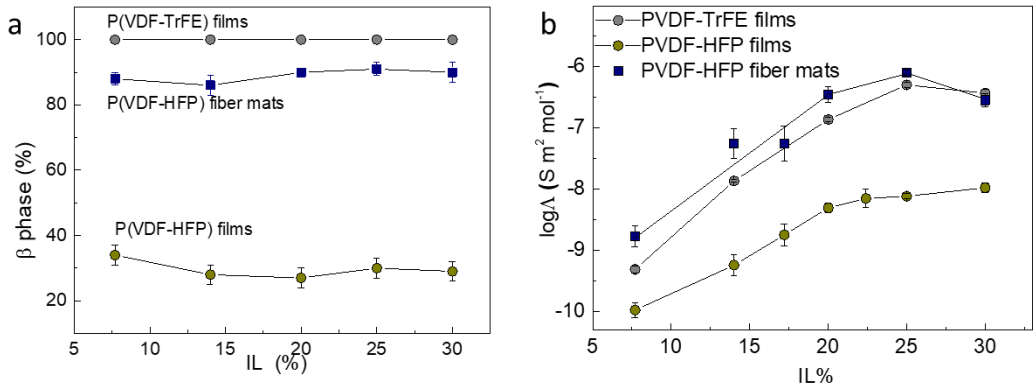

Fig. S15 (a) β-phase content and (b) molar conductivity of P(VDF-TrFE) films, P(VDF-HFP) films and fiber mats with different IL content.

Table S1. Summary of the characteristics of PVDF and copolymer-based nanofiber in this work and other reported studies

Material	Output voltage	Force (N)/Pressure(Pa)	Reference
PVDF	1.3 V	Not quantified	S7
PVDF/LiCl	5.0 V		
PVDF	3.8 V	Not quantified	S8
PVDF/graphene	7.9 V		
PVDF	2.6 V	10 N	S9
PVDF	2.2 V	10 N	S10
PVDF	2.0 V	Not quantified	S11
PVDF/MWCNTs	6.0 V		
PVDF-HFP/$AgNO_3$	3 V	15 kPa	S12
PVDF-HFP/ Eu^{3+}	5 V	5.6 kPa	S13
PVDF-HFP/ Eu^{3+}/ graphene	9 V		
PVDF-TrFE	9 V	Not quantified	S14
PVDF-TrFE/ MWCNTs	18.23 V		
PVDF-TrFE	10 V	30 kN	S15
P(VDF-HFP)	2.5 V	24 N	This work

Note S5. Temperature calculation from the resistance change of ionic thermistors

The resistance change of the ionic thermistor is not linear with temperature, instead, lnσ is linear with 1/T (as shown in Fig. S16a). According to Arrhenius equation ($\sigma = \sigma_0 \exp(-\frac{E_a}{k_b T})$), the slope of the plotted lnσ is related to the activation energy of the sample. From the linear relation, we derived the correlation between the measured resistance changes to the temperature as below:

$$\frac{1}{T} = \frac{1}{T_0} + \frac{ln\frac{R}{R_0}}{\frac{E_a}{k_B}} \qquad \text{(S5)}$$

The "TCR" of a thermistor is defined as $TCR = \frac{dR}{dT}\frac{1}{R}$, since $lnR = lnR_o + \frac{eE_a}{k_B T}$, $TCR = \frac{eE_a}{k_B T^2}$. The TCR of fiber mats and films with different IL contents are shown in Fig. S16b.

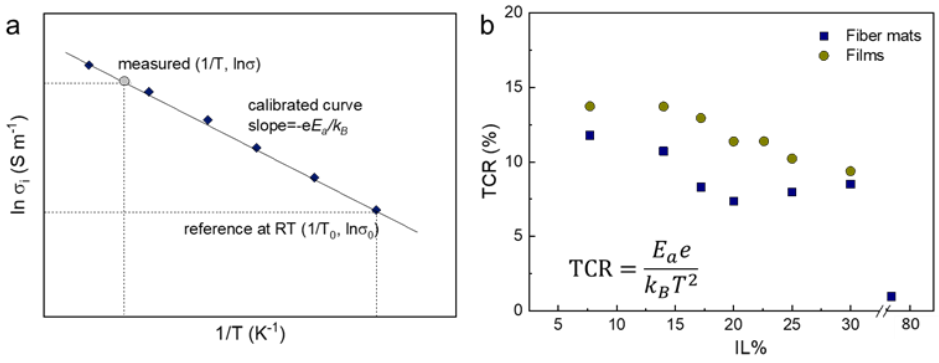

Fig. S16 (a) Illustration of the calculation and (b) the TCR of electrospun fiber mats and films with different IL content from the data recorded with impedance spectrometer.

References

[S1] S. K. Ghosh, M. M. Alam and D. Mandal, *RSCAdv*., 2014, **4**, 41886–41894.

[S2] A. Sultana, P. Sadhukhan, M. M Alam, S. Das, T. R. Middya and D. Mandal, *ACS Appl. Mater. Interfaces*, 2018, **10**, 4121–4130.

[S3] E. Shaulsky, S. Nejati, C. Boo, F. Perreault, C. O. Osuji and M. Elimelech, *J. Membr. Sci*., 2017, **530**, 158–165.

[S4] O. Larsson, E. Said, M. Berggren and X. Crispin, *Adv. Funct. Mater*., 2009, **19**, 3334–3341.

[S5] J. Y. Song, Y. Y. Wang and C. C. Wan, *J. Power Sources*, 1999, **77**, 183–197.

[S6] Y. Cao, T. G. Morrissey, E. Acome, S. I. Allec, B. M. Wong, C. Keplinger, and C. Wang, *Adv. Mater*. 2017, **29**, 1605099.

[S7] F. Mokhtari, M. Shamshirsaz, M. Latifi and J. Foroughi, *Polymers*, 2020, **12**, 2697.

[S8] M. M. Abolhasani, K. Shirvanimoghaddam and M. Naebe, *Compos. Sci. Technol*., 2017, **138**, 49–56.

[S9] J. Fang, H. Niu, H. Wang, X. Wang and T. Lin, *Energy Environ. Sci*., 2013, **6**, 2196–2202.

[S10] H. Shao, J. Fang, H. Wang and Tong Lin, *RSC Adv*., 2015, **5**, 14345–14350.

[S11] H. Yu, T. Huang, M. Lu, M. Mao, Q. Zhang and H. Wang, *Nanotechnology*, 2013, **24**, 405401.

[S12] D. Mandal, K. Henkel and D. Schmeißer, *Phys. Chem. Chem. Phys*., 2014, **16**, 10403–10407.

[S13] P. Adhikary, A. Biswas and D. Mandal, *Nanotechnology*, 2016, **27**, 495501.

[S14] C. Zhao, J. Niu, Y. Zhang, C. Li, P. Hu, *Compos. B. Eng*., 2019, **178**, 107447.

[S15] M. Zhu, S. S. Chng, W. Cai, C. Liu and Z. Du, *RSC Adv*., 2020, **10**, 21887–21894.